This full text paper was peer-reviewed at the direction of IEEE Instrumentation and Measurement Society prior to the acceptance and publication.

Experimental investigation of gas-oil two-phase flow using electrical capacitance tomography

Yinyan Liu[1,2], Yuchi Deng[1,2] and Yi Li[1*]
[1] Graduate School at Shenzhen, Tsinghua University, Shenzhen 518055, China
[2] Department of Automation, Tsinghua University, Beijing 100084, China.
liyi@sz.tsinghua.edu.cn

***Abstract*—An 8-electrode electrical capacitance tomography (ECT) sensor located at the venturi throat on a vertical pipeline is used to investigate the flow regime of gas-oil two-phase flow. The experiment was carried out with the gas volume fraction (GVF) varies from 10% to 90% at different flow rates of oil. Slug flow appears at a low GVF. While with a high GVF, a clear annular flow will be formed. For different flow rates of oil, the flow regime at the same GVF point could be different because of the flow rate of gas (or superficial velocity of gas). A method independent of flow regime is developed to calculate the phase fraction of gas-oil two-phase flows. The absolute error can be within ±10%, illustrating that this method is effective.**

Keywords—gas-oil two-phase flows, electrical capacitance tomography, phase fraction measurement.

I. INTRODUCTION

It is well known that the gas-oil two-phase flow widely exists in the industrial processes. Online phase fraction measurements without separating the mixture are crucial to ensure the safety and efficiency of industrial production and management [1]. Different from single-phase flow, gas-oil two-phase flow with rheological complexity of the coupling effect of gas and oil presents different flow regimes, such as bubble flow, slug flow, annular flow, stratified flow and so on [2]. That makes the accurate phase fraction (i.e. gas volume fraction, GVF) measurement of gas-oil two-phase flow a significant challenge.

A number of techniques have been proposed to calculate phase fraction of multiphase mixtures, such as quick closing valves (QCV), radiation methods, microwave methods and electrical methods, etc. QCV is suitable for steady-state measurements with the advantages of low cost, simple operation and reliability [3]. However, it is an off-line method and limited by the non-continuous measurement. Radiation methods including α-ray, x-ray, γ-ray and so on, are widely used as a nonintrusive and highly accurate method. While because of the radiation, the adaption range of those methods are limited [4]. The microwave methods measuring the holdup based on the different permittivity between oil and gas phases are sensitive to noises and high-cost [5]. Meanwhile, because of low cost, fast and simple superiority, electrical capacitance tomography (ECT) [6] [7] has been widely applied in various industrial process applications for real-time measurement.

An important application of ECT is viewing and measuring the spatial distribution of a dielectric mixture, e.g. gas-oil two-phase flow [8], gas-water two-phase flow [9] and gas-oil-water three-phase flow [10]. The electrical property of oil and gas differ from each other, *i.e.* oil is normally of high permittivity compared with gas. Therefore, gas-oil mixtures of different phase fraction have different electrical capacitance measurements.

One general gas-oil two-phase flow phase fraction measurement method is a flow regime identification method, which recognizes flow regime firstly, and then calculates phase fraction based on different flow regimes [11] [12]. This method requires an accurate identification of flow regimes and is time consuming and complex. Thus, it is highly attractive to develop a method to predict the phase fraction independent of the flow regimes.

In this work, using the non-intrusive electrical capacitance tomography, we focus on investigating the flow regime varies with different gas and oil flow rate and calculating the phase fraction of the gas-oil two-phase flow independent of flow regimes and phase fraction range.

II. METHODOLOGY

ECT provides a non-intrusive way to visualize the permittivity distribution of dielectric materials by measuring the changes in capacitance over the electrode pairs. Typically the N electrodes of an ECT sensor evenly installed on the external surface of an insulating pipe (see Figure 1) [13]. Each electrode can be configured to act as a transmitter or detector. When one of the electrodes is excited in turn and other electrodes are kept at zero potential, the number of independent capacitance measurements will be N(N-1)/2 [6].

978-1-5386-1620-8/17/$31.00 ©2017 IEEE

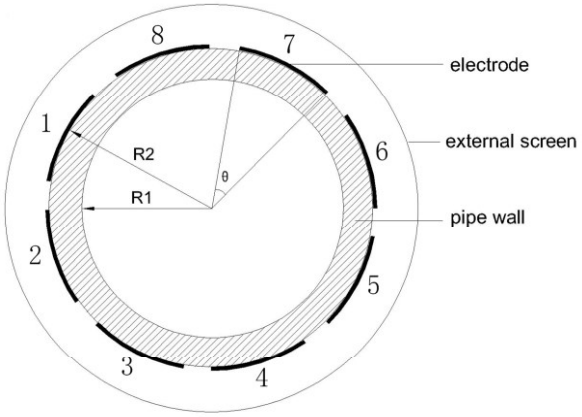

Figure 1. 8-electrode ECT sensor.

In ECT, the boundary conditions are the electrical potential distribution $\phi = V$ for excited electrode and $\phi = 0$ for rest electrodes. In two-dimensional geometry, the relationship between the capacitance C and the permittivity distribution can be expressed as [6]:

$$C = \frac{Q}{V} = -\frac{1}{V}\iint_{\Gamma} \qquad \nabla \qquad \Gamma \quad (1)$$

where Q is the electric charge, $\varepsilon(x, y)$ and $\phi(x, y)$ are the permittivity distribution and the potential distribution in the sensing area respectively, Γ is the electrode surface and ∇ represents a gradient operator.

For an 8-electrode ECT sensor, 28 independent measurement can be obtained, which will be typically grouped as adjacent-pair, one-electrode apart, two-electrode apart and opposite-pair measurement according to the spatial distance between the excited electrode and the measured electrode [14].

To minimize the impact of noise due to the screen, the pipe wall and the cables, appropriate calibration strategies should be applied on raw capacitance measurements. In this work, the normalized capacitance C_n can be obtained by [15]:

$$C_n = \frac{C_m - C_l}{C_h - C_l} \quad (2)$$

where C_m is the raw capacitance of gas-oil two-phase flow, C_l is the capacitance of low calibration point obtained from an empty pipe with a relative dielectric constant $\varepsilon_r = \varepsilon_{air} = 1.0$, and C_h is the capacitance when the pipe filled with oil, the relative dielectric constant $\varepsilon_r = \varepsilon_{oil}$ is 2.2. Following this process, the normalized capacitance values can represent the capacitance changes between the measurement of gas-oil mixture and the measurement of empty pipe.

For dielectric medium, ECT can be used to reconstruct the permittivity distribution from capacitance measurements. In this work, the reconstructed image determined by the capacitance changes can be seen as the presence of difference materials. Thus, the reconstructed permittivity can represent the phase fraction of the pipe cross section. Linear back projection (LBP) is used to obtain the permittivity distribution of the gas-oil two-phase flow [16]:

$$g = \frac{S^T C_n}{S^T \mu_1} \quad (3)$$

where g is the reconstructed image, S is normalized sensitivity matrix of ECT, and μ_1 is the identity vector, i.e. $\mu_1 = [1, 1, 1, \cdots$.

To develop a phase fraction measurement method independent of the flow regimes, the reconstructed permittivity is used to calculate the phase fraction, i.e. GVF. In this work, the resolution of reconstruction image is 64 x 64, of which 3196 pixels are valid since the image region is circle. The phase fraction of gas, GVF is calculated as follow:

$$GVF = 1 - \frac{\sum_{i=1}^{n} g_i}{n} \quad (4)$$

where g_i is the reconstructed permittivity of ith pixel and n is 3196. This equation is based on the hypothesis that the phase fraction is proportional to the permittivity [17]. So if the pipe is full of oil (GVF=0%), the reconstructed permittivity should be 1 based on the calibration formula used in this work. For instance, if the permittivity is 0.6 in one pixel, the phase fraction of oil is 60%, namely GVF=40%.

III. Experiment

The experiments were carried out on the gas-oil-water multiphase flow facility in Graduate School at Shenzhen, Tsinghua University. As described in **Figure 2** (a), oil and water stored in the separator can be simply separated based on gravity principle. The pipelines shown in blue color represent the single phase of gas, oil and water. Oil and water are pumped from the separator and gas phase will be generated from gas compressor. Thus three-phase mixture can pass through the horizontal or vertical test line (in gray color, size of 2, 3 or 4 inches'). The length of test line is designed as 8 meters. Different sensor sections, e.g. ECT or ERT can be located on the test line. The maximum pressure that the facility can hold is up to 2.4 Mpa.

In this work, an ECT sensor with 8 electrodes was located on the venturi throat section where the inner diameter is 30mm (see **Figure 2** (b)), and installed outside a 5 mm thick insulating pipe liner made from PEEK (relative dielectric constant $\varepsilon_r \approx 3.2$). An AC-based data acquisition system is used to take measurements from ECT sensor [18]. The data sampling rate are about 50 frames/s. The excitation signal frequency is 500 kHz. And the signal-to-noise ratio of the hardware system is around 62dB.

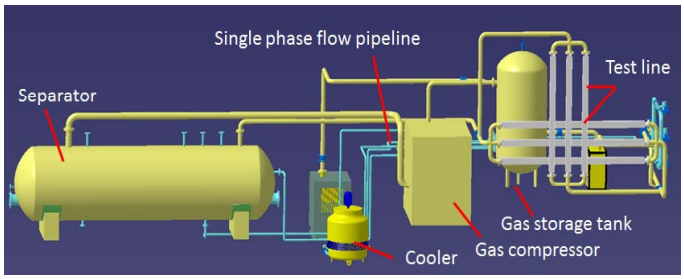

(a) Schematics of Multiphase flow facility

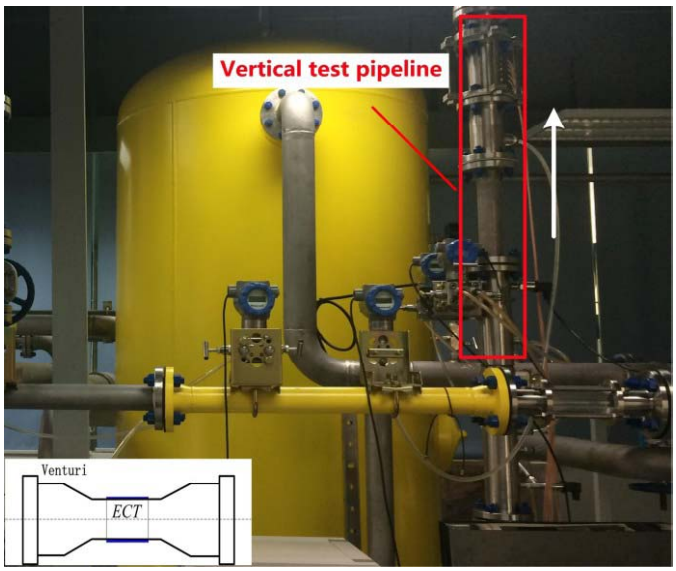

(b) ECT test section of gas-oil two-phase flow

Figure 2 Multiphase flow facility and ECT test section

Experiments with different flow rates and GVF were tested in vertical pipeline. The experimental materials were technical white oil with relative permittivity density = 880 kg/m^3 and viscosity = 8.8 mPa· s (32℃). The working pressure is set to 0.6 Mpa and temperature of the flows is about 32 degree centigrade obtained by a temperature transmitter. The flow rate of oil Q_{oil} was fixed in several values through our experiments: 3, 4, 6 m^3/h. Then with the fixed flow rate of oil, the flow rate of gas Q_{gas} adjusted to reach varying GVF. The sampling time for each test point was 60 seconds. The experimental conditions are summarized in Table I, where Q_{gas} is estimated under working condition.

TABLE I. TEST MATRIX

Q_{gas} (m^3/h)			GVF
Q_{oil} =3m^3/h	Q_{oil} =4m^3/h	Q_{oil} =6m^3/h	
0.40	0.38	0.75	10%
1.32	1.61	2.88	30%
3.50	4.80	6.50	50%
6.72	8.60	15.3	70%
24.7	29.5	57.1	90%

IV. RESULTS AND DISCUSSION

To investigate the flow regime of gas-oil flow, instantaneous longitudinal tomographic images are reconstructed under various experimental conditions. **Figure 3** shows the results obtained from 3000-frame continuous data for each experimental condition as summarized in Table I.

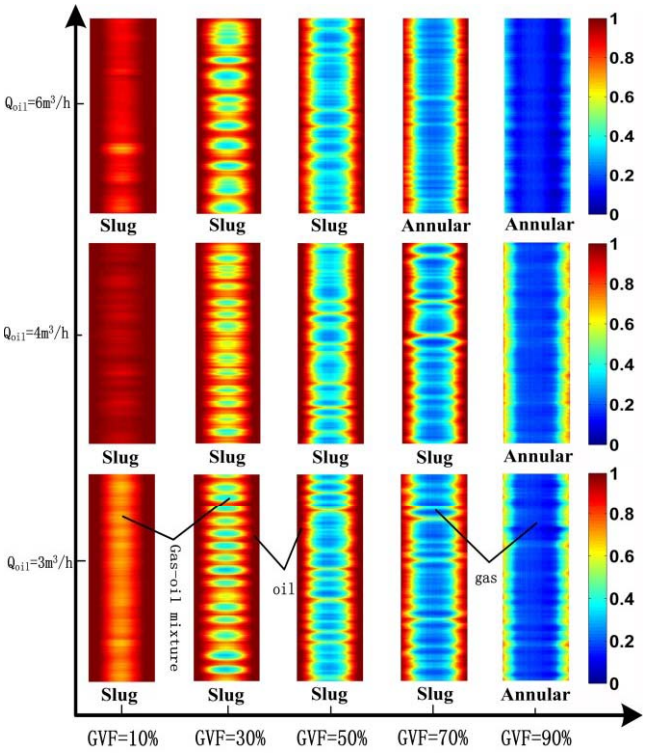

Figure 3. Instantaneous longitudinal images of gas-oil two-phase flows under different experimental conditions based on LBP.

Note that for a fixed flow rate of oil, the flow regime varies with the increase of GVF. The gas-oil flow presents slug with a low GVF, say GVF is less than 90% for Q_{oil}=3 or 4m^3/h and 70% for a higher flow rate, say Q_{oil}=6m^3/h. When GVF is 10%, the color of the reconstructed image of GVF=10% is relatively homogeneous indicates that tiny gas bubbles are dispersed in the liquid stream. With the increase of GVF, a clear slug flow appeared in the pipe that large bubbles of gas with a diameter less than the diameter of pipeline occur at the cross section. The larger the GVF is, the clearer and more frequent the bubble will be. With a further increase of GVF, a symmetrical gas core is obtained in the middle of pipe, which means the annular flow forms when the gas flows at high speed. In this work, it occurs at the point of GVF=90% for Q_{oil}=3 and 4m^3/h, and GVF>70% for Q_{oil}=6m^3/h. No matter slug flow or annular flow, there is a thin oil layer adhering to the wall of the pipe.

As shown in **Figure 3**, the flow regime may varies with different flow rates of oil at the same GVF point. When GVF is 70%, the flow regime is slug for Q_{oil}=3 and 4m^3/h, and annular for Q_{oil}=6m^3/h. This is because there is a higher flow rate of gas for Q_{oil}=6m^3/h than Q_{oil}=3 and 4m^3/h even though with the same GVF. From Table I, it can be seen that the flow rates of gas are 6.72m^3/h for Q_{oil}=3m^3/h, 8.60m^3/h for Q_{oil} =4m^3/h and

15.3m^3/h for Q_{oil}=6m^3/h with GVF=70%. The flow rate of gas for Q_{oil}=6m^3/h is nearly two times of that for Q_{oil}=3 or 4m^3/h. Thus, with different Q_{oil}, the flow regime not only determined by GVF but also influenced by the flow rate of gas (or superficial velocity of gas).

Figure 4 shows the time-average normalized capacitance results of different measurement groups against Q_{gas}. To reduce the inhomogeneous of gas-oil flow, spatial average of different measurement groups is used in this work.

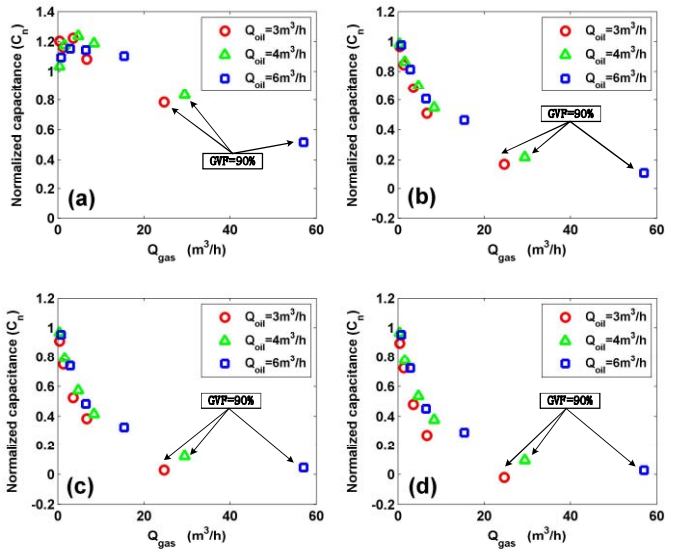

Figure 4. 60 seconds time-average normalized capacitance C_n against flow rate of gas Q_{gas} with different spatial average electrode pairs: (a) adjacent pair (b) one-electrode apart. (c) two-electrode apart, (d) opposite pair.

Note that the measurements of different Q_{oil} have no significant different when Q_{gas} is less than 10m^3/h, meaning that the flow rate of oil has little effect on the flow regime at low GVF. This is consistent with the reconstructed images for GVF is less than 70% as illustrated in **Figure 3**. For GVF=90%, the measurements of one-electrode apart pair, two-electrode pair and opposite pair almost the same with different Q_{oil}. While the adjacent-pair measurements of Q_{oil}=6m^3/h are significantly smaller than that of Q_{oil}<4m^3/h. This phenomenon also can clearly be identified from the differences of reconstructed images shown in **Figure 3**. When GVF is 90%, a large gas core is in the middle of the pipe. The measurements of one-electrode apart, two-electrode apart and opposite pairs mainly affected by the gas. It presents that the normalized capacitances C_n are zero, roughly. However, the measurement adjacent electrode pair mainly covers a little area "near wall", which leads the measurements are mainly determined by the thick of oil layer. The thicker of the oil layer is, the larger the adjacent-pair capacitance measurement. Therefore, the thick of oil layer for Q_{oil}=6m^3/h is smaller than that for Q_{oil}≤4m^3/h even though they have the same GVF (say 90%). This is mainly because of the influence of flow rate of gas (or superficial velocity of gas).

Figure 5 illustrates the relationship of normalized capacitance against the reference GVF for different measurement groups. It is found that an approximate linear relationship can be seen from the one-electrode apart, two-electrode apart and opposite pair measurements (see **Figure 5** (b), (c) and (d)). This is because that the flow regime is nearly symmetrical slug or annular flow (see **Figure 3**). Since the adjacent electrode pair measurements mainly cover the near-wall region where a thin oil layer adhering, so the normalized capacitances of adjacent electrode pair almost have no change from GVF=10% to GVF=70%, this phenomenon suggests that using "near-wall" capacitance to derive the water-to-liquid ratio of the gas-oil-water three-phase flow might be promising. When GVF is 90%, a sudden drop of adjacent pair measurements since the oil layer becomes much thinner with a high gas speed. Besides, as shown in **Figure 5**(d), the linearity between the GVF and capacitance measurements predicts that using opposite-pair measurements to derive the GVF of gas-liquid multiphase flows is suggested.

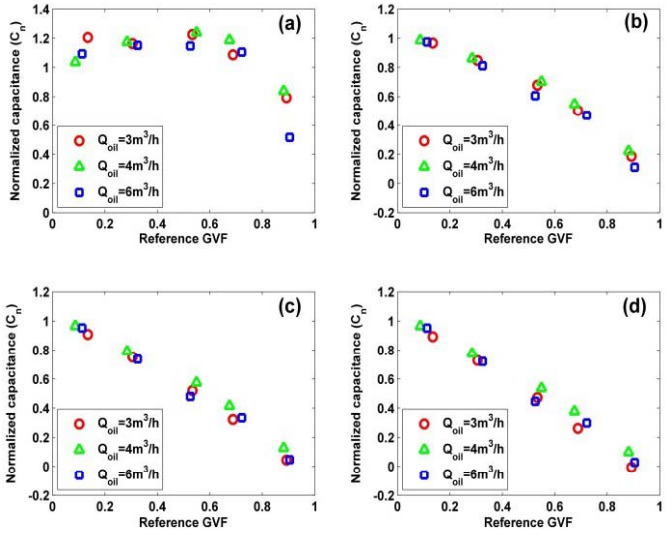

Figure 5. 60 seconds time-average normalized capacitance C_n against reference GVF with different spatial average electrode pairs: (a) adjacent pair (b) one-electrode apart. (c) two-electrode apart. (d) opposite pair.

From above analysis, we know that the flow regime of gas-oil flow is affected by both the flow rate of gas and the flow rate of oil. Equation (4) is used to calculate the gas volume fraction. It is independent of the flow regime. **Figure 6** shows the calculated results based on time-average measurements. The absolute error can keep within ±10%. The calculated GVF are less than the reference values when GVF<50%. While the calculated results are larger than the reference GVF for GVF=90%. This might because the calculated results based on image reconstruction represent the phase fraction of cross section rather than the phase fraction of volume. As shown in **Figure 3**, the phase fraction of cross section might varies with the speed of gas even at the same GVF. Thus, a further research about how the speed of gas impact the flow regime and phase fraction measurements should be developed in the future.

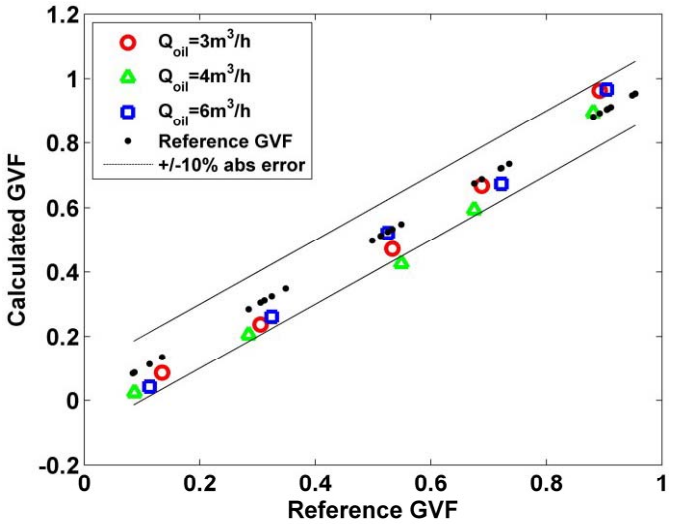

Figure 6. Calculated GVF against reference GVF based on image reconstruction.

V. Conclusions and Discussion

This paper investigated the flow regime of gas-oil two-phase flow with different flow rate. Slug flow appears at a low GVF point, say GVF is less than 90% for Q_{oil}<4m^3/h and 70% for Q_{oil}=6m^3/h. While with a higher GVF, a clear annular flow will be formed. A symmetrical gas core is obtained in the middle of pipe with a thin oil layer adhering the wall. For different flow rate of oil, the flow regime at the same GVF point might be different, this is because that a high flow rate of gas will also affects the flow regime. Phase fraction of gas-oil two-phase flow was calculated by a method independent of flow regime. The absolute error can be within ±10%, showing the capability of electrical capacitance tomography for gas-oil two phase flow measurement. Future work will focus on (1) experimental investigation of gas-oil two-phase flow in horizontal pipeline, (2) The effects of superficial velocity of gas on the flow regime and phase fraction measurement.

Acknowledgment

The authors would like to thank the National Natural Science Foundation of China (No.61571252) and the Shenzhen government support grant (KQCX2015033111358159) for supporting this work.

References

[1] Plaskowski A, Beck M S, Thorn R, et al. Imaging Industrial Flows: Applications of Electrical Process Tomography [J]. Applied & Industrial Physics, 1995.

[2] Banasiak R, Wajman R, Jaworski T, et al. Study on two-phase flow regime visualization and identification using 3D electrical capacitance tomography and fuzzy-logic classification [J]. International Journal of Multiphase Flow, 2014, 58: 1-14.

[3] Xue Y, Li H, Hao C, et al. Investigation on the void fraction of gas–liquid two-phase flows in vertically-downward pipes [J]. International Communications in Heat & Mass Transfer, 2016, 77:1-8.

[4] Teniou S, Meribout M. Multiphase flow meters principles and applications: a review [J]. Can. J. Sci. Ind. Res, 2011, 2(8): 290-293.

[5] Xie C G. Measurement Of Multiphase Flow Water Fraction And Water-cut [J]. Aip Conference Proceedings, 2007, 914(1):232-239.

[6] Xie C G, Huang S M, Hoyle B S, et al. Electrical capacitance tomography for flow imaging: system model for development of image reconstruction algorithms and design of primary sensors [J]. Circuits Devices & Systems Iee Proceedings G, 1992, 139(1):89-98.

[7] Ismail I, Gamio J C, Bukhari S F A, et al. Tomography for multi-phase flow measurement in the oil industry [J]. Flow Measurement & Instrumentation, 2005, 16(2–3):145-155.

[8] Zhang L, Wang H. Identification of oil–gas two-phase flow pattern based on SVM and electrical capacitance tomography technique[J]. Flow Measurement & Instrumentation, 2010, 21(1):20-24.

[9] Ismail I, Shafquet A, Karsiti M N. Void fraction estimation by using electrical capacitance tomography and differential pressure in an air–water co-current bubble column [J]. Aust. J. Basic Appl. Sci., 2011, 5(11): 1533-1541.

[10] Li Y, Yang W, Wu Z, et al. Gas/oil/water flow measurement by electrical capacitance tomography[C]//Imaging Systems and Techniques (IST), 2012 IEEE International Conference on. IEEE, 2012: 83-88.

[11] Xie D, Huang Z, Ji H, et al. An Online Flow Pattern Identification System for Gas–Oil Two-Phase Flow Using Electrical Capacitance Tomography [J]. IEEE Transactions on Instrumentation & Measurement, 2006, 55(5):1833-1838.

[12] Salgado C M, Pereira C M N A, Schirru R, et al. Flow regime identification and volume fraction prediction in multiphase flows by means of gamma-ray attenuation and artificial neural networks [J]. Progress in Nuclear Energy, 2010, 52(6):555-562.

[13] Yang W. Design of electrical capacitance tomography sensors [J]. Measurement Science & Technology, 2010, 21(4):447-453.

[14] Ye J, Yang W. Evaluation of Electrical Capacitance Tomography Sensors for Concentric Annulus [J]. IEEE Sensors Journal, 2013, 13(2):446-456.

[15] Li Y, Yang W, Xie C, et al. Gas/oil/water flow measurement by electrical capacitance tomography [J]. Measurement science and technology, 2013, 24(7): 074001.

[16] Yang W Q, Peng L. Image reconstruction algorithms for electrical capacitance tomography [J]. Measurement science and technology, 2002, 14(1): R1.

[17] Huang Z, Wang B, Li H. Application of electrical capacitance tomography to the void fraction measurement of two-phase flow [J]. IEEE Transactions on Instrumentation & Measurement, 2003, 52(1):7-12.

[18] Yang W Q, York T A. New AC-based capacitance tomography system [J]. Science, Measurement and Technology, IEE Proceedings -, 1999, 146(1):47-53.